Plant VAP27 proteins: domain characterization, intracellular localization, and role in plant development.

Pengwei Wang[1], Christine Richardson[1], Tim J Hawkins[1], Imogen Sparkes[3], Chris Hawes[2] and Patrick J Hussey[1]*

1. School of Biological and Biomedical Sciences, Durham University, South road, Durham, DH1 3LE, UK

2. Department of Biological and Biomedical Sciences, Oxford Brookes University, Gipsy lane, Oxford, OX3 0BP, UK

3. College of Life and Environmental Sciences, University of Exeter, Stocker road, Exeter, EX4 4QD, UK

* Corresponding author: p.j.hussey@durham.ac.uk; Tel: +44(0)1913341335; Fax: 44(0)1913341201

Summary (200 words)

- The endoplasmic reticulum (ER) is connected to the plasma membrane (PM) through the plant specific NETWORKED protein, NET3C, and phylogenetically conserved Vesicle-Associated Membrane Protein-Associated Proteins (VAPs).
- Ten VAP homologues (VAP27-1 to 10) can be identified in the Arabidopsis genome and can be divided into three clades. Representative members from each clade have been tagged with fluorescent protein and expressed in *Nicotiana benthamiana*.
- Proteins from clades one and three localised to the ER as well as to ER/PM contact sites (EPCS), whereas proteins from clade two are found only at the PM. Some of the VAP27 labelled EPCS localised to plasmodesmata, and we show that the mobility of VAP27 at the EPCS is influenced by the cell wall. EPCS closely associate with the cytoskeleton, but their structure is unaffected when the cytoskeleton is removed.
- VAP27 labelled EPCS are found in most cell types in Arabidopsis with the exception of cells in early trichome development. Arabidopsis expressing VAP27-GFP fusions exhibit pleiotropic phenotypes including defects in root hair morphogenesis. A similar effect is also observed in plants expressing VAP27 RNAi.
- Taken together these data indicate that VAP27 proteins used at the EPCS are essential for normal ER-cytoskeleton interaction and for plant development.

Key words:

ER/PM contact sites, endoplasmic reticulum, VAP27, Scs2, NET super-family

Introduction

Proteins and other cargos synthesised in the ER are transported to various destinations through the conventional vesicular trafficking pathway. In higher plants, the cortical endoplasmic reticulum (ER) network is a highly dynamic structure and its movements are regulated by the actin cytoskeleton in most cell types (Boevink *et al.,* 1998; Sparkes *et al.,* 2009b). However, direct association between the ER and other membrane compartments also exists (Stefano *et al.,* 2014; Hawes *et al.,* 2014), which may provide alternative transport routes, a so-called non-vesicular pathway. These may include the ER-Golgi interface (daSilva *et al.,* 2004; Hawes *et al.,* 2008; Sparkes *et al.,* 2009a), an ER-chloroplast (Mehrshahi *et al.,* 2014) connection and ER/PM contact sites (Sparkes *et al.,* 2009b, Manford *et al.,* 2012; Wang *et al.,* 2014).

Various ER/PM contact sites (EPCS) have been reported in different species, and are regulated by various proteins. For example, the STIM1/Orai1 complex is found in animals and is required for intercellular calcium transport (Varnai *et al.,* 2007; Carrasco and Meyer 2011). In yeast, the Scs2/Osh/Sac complex is found at the ER and is used for lipid transfer to the PM (Stefan *et al.,* 2011; Loewen *et al.,* 2005). This complex also regulates ER morphology during budding (Loewen *et al.,* 2007). A few other candidates such as Ist2 and Tlb (known as synaptotagmins in animals and plants) have also been identified as candidates for regulating the formation of the EPCS (Manford *et al.,* 2012; Perez-Sancho *et al.,* 2015). In plants, early electron microscopy studies described the structure of the EPCS (Hepler *et al.,* 1990), and persistency mapping identified these structures in living cells (Sparkes *et al.,* 2009b). However, their protein composition has not been fully elucidated and recent studies have begun to redress this situation (VAP27/NET3C complex, Wang et al., 2014).

The ER/PM contact site is linked to the cytoskeleton and this is mediated by a VAP27/NET3C complex through its interactions with microtubules and F-actin (Wang *et al.,* 2014). A similar association between the cytoskeleton and EPCS has also been reported in migrating cancer cells, where the ER/PM junction is formed at the leading edge and is associated with actin markers (Dingsdale *et al.,* 2013). Therefore, it is likely that the close association between EPCS and the cytoskeleton is important for cell polarity and development.

Vesicle-Associated Membrane Protein (VAMP) - Associated Proteins (VAP) are conserved amongst phylogentically distinct organisms, and were first identified in the SNARE protein complex that is involved in vesicle docking and fusion (Skehel *et al.,* 1995). Their plant homologues are named VAP27 because the first member identified had a molecular weight of 27 kDa (Laurent *et al.,* 2000). As the name suggests, animal VAPs bind to a wide range of SNARE proteins that are required for vesicle trafficking from the ER (Weir *et al.,* 1998; Weir *et al.,* 2001; Soussan *et al.,* 1999). Their functions in lipid transfer have been well studied in yeast, and similar functions are likely to exist in plants due to the identification of their interaction with oxystereol-binding proteins (ORPs) and sphingolipid transfer proteins (Saravanan *et al.,* 2009; Petersen *et al.,* 2009). In addition, recent studies have shown that VAPs are also required in the virus infection pathway, which is unique to plants (Barajas *et al.,* 2014).

Plant EPCS can be defined as persistent ER nodes/punctae that are static whilst the ER remodels (Sparkes et al., 2009b), as well as sites where ER membrane attach to the PM as observed in ultrastructural studies (Hepler et al., 1990). In this study, we use either VAP27-1-YFP or GFP-NET3C as markers for EPCS in plants (Wang et al., 2014, Perez-Sancho *et al.,* 2015; Levy et al., 2015). We identify ten VAP homologues in the Arabidopsis genome, all of which contain a highly conserved major sperm domain (Laurent *et al.,* 2000). We have chosen members of each of the three phylogenetic clades to study their intracellular localization, functional domains and effects on plant development.

Materials and Methods

Bioinformatic analysis

Multiple alignments were assembled in ClustalX (Larkin et al. 2007) and exported as graphics using Jalview. Domains were identified with the Simple Modular Architecture Research Tool, SMART (Schultz et al. 1998), Interpro (Hunter *et al.,* 2011) Coils (Lupas *et al.,* 1991) and TMHMM (Sonnhammer *et al.,* 1998). The Maximum likelihood method was chosen for the VAP family phylogenetic tree as this method has been identified as one of the most robust optimality criterion. Maximum Likelihood trees were calculated in the MetaPIGA software

package (Helaers and Milinkovitch, 2010), using stochastic heuristics for large phylogeny inference with the Metapopulation Genetic Algorithm (metaGA) (Lemmon and Milinkovitch, 2002). MetaGA is an evolutionary computation heuristic in which several populations of trees exchange topological information which is used to guide the Genetic Algorithm (GA) operators for much faster convergence. MetaPIGA calculations were stopped when the mean relative error of 10 consecutive consensus trees stayed below 5% using trees sampled every 5 generations or the Likelihood stopped increasing after 200 iterations. Trees were drawn and exported as graphical files from FigTree (Andrew Rambout, University of Edinburgh). Transcription profiles of VAP isoforms were generated with Gene Investigator (Zimmermann et al. 2004, NEBION / ETH Zurich) from publicly available DNA microarray data.

Molecular biology

Primers and plasmids used in vector constructions are listed in Supplementary table 1. The VAP27 full-length cDNAs were amplified by RT-PCR (Invitrogen, UK) with gene specific primers (Table S1). Fluorescent protein fusions to VAPs were made using Gateway recombination (Invitrogen) into various destination vectors as shown in Table S2. Full length VAP27s, as well as the major sperm, coiled-coil and transmembrane domain deletion mutants of VAP27-1 and 3, were generated using PCR with appropriate primers. The VAP27-3 Arabidopsis RNAi line was obtained from AGRIKOLA (Hilson *et al.*, 2004) and the RNAi insertion was confirmed using AGRIKOLA specific primers (Table S1). The VAP27-1 RNAi construct obtained from AGRIKOLA was sub-cloned into the pHELLSGATE RNAi vector (Wesley *et al.,* 2001) and transformed into *Col-0* Arabidopsis.

Plant transformation and GUS study

Arabidopsis (Col-0) was grown on compost in a growth chamber with a 16hr light (22 °C) and 8hr dark (18 °C) regime. *N. benthamiana* were maintained in a growth room with a 16hr light (25°C) and 8hr dark (18°C) regime. Transient expression was performed by leaf infiltration using *N. benthamiana* with Agrobacterium (Sparkes *et al.,* 2006). Stable transformed *Arabidopsis* lines were generated using floral-dipping (Zhang *et al.,* 2006). The VAP27-1 and 3 genomic sequences (including promoter and open reading frame) were fused

in frame (without the termination codon) to the 5' end of the GUS reporter sequence. Stable GUS plants were obtained by selecting floral-dipped seeds on half MS medium containing kanamycin. GUS staining and histological studies were performed as described in Deeks *et al.,* 2012.

Antibodies and Immunofluorescence study

VAP27-1 cDNA corresponding to amino-acid residues 164-230 was cloned into pET28a plasmid (Novagen) which incorporates an N-terminal His tag into the expressed protein (see supplementary 1 for primers used). Recombinant proteins were generated in *E.coli* (Rosseta 2, Novagen) and purified using nickel agarose beads (Qiagen). Polyclonal antibodies were raised in mice as described (Ketelaar *et al.,* 2004). The specificity of the antiserum was tested on a one dimensional gel western blot of a total protein extract from 14 day old Arabidopsis seedlings. For detection, the membrane was incubated in TBST buffer with 5% milk prior to primary antibody incubation (1:500-1000) and HRP-conjugated secondary ant-imouse IgG (1:3000) and developed using the ECL reagent (GE Heathcare). PageRuler pre-stained protein ladder (Life technologies) was included on the western blot. Immunofluorescence with freeze shattering was performed as described (Zhang et al., 2013). Antibodies were diluted and used at 1:300 for VAP27 and 1:500 for BIP2 (Agrisera), followed by secondary antibody incubation with TRITC-conjugated anti-mouse IgG and FICT-conjugated anti-rabbit (Jackson ImmunoResearch).

Confocal microscopy and live cell imaging

All the microscopy images in this paper are representative of more than three independent infiltrations or stable transformations.

Samples were imaged using laser scanning confocal microscopes (LSCM, Leica SP5). Images were taken in multi-track mode with line switching when multi fluorescence was used. FRAP experiments and data analyses were performed as described (Wang *et al.,* 2011), using a minimum number of 15 areas of interest which were bleached from different cells. During the photobeaching step, full output from the laser line was used and low laser intensities (1% 514nm for YFP) were used for data collection. The difference in maximum recovery was analyzed using the Student's t-test to confirm the statistical significance. FRET-

FLIM analysis was performed as described (Wang *et al.,* 2014), 12 repetitions were performed for each sample. Protoplasts were prepared using infiltrated leaves of *N. benthamiana*. Leaves were cut with a blade every 2mm and placed in a petri dish containing enzyme mix (macerozyme 0.2%, cellulose 0.4%) with K3 buffer (B5 basal medium 3.78g/l; $CaCl_2$ 750mg/l; NH_4NO_3 250mg/l; sucrose 136.2/l; xylose 250mg/l; 6-benzylaminopurine 1mg/l; Naphtalenacetic acid 1mg/l). Digestion was carried out over-night at room temperature. The enzyme mix was removed the next day, and cells were suspended in K3 buffer for microscopy studies. Cell wall as stained with calcofluor as described (Martiniere *et al.,* 2011). Plasma membrane staining was performed by immersing small leaf segments into water solution containing FM4-64 (7.5µm, Sigma) for 10min. Plasmodesmata were labeled using aniline blue as described (Deeks *et al.,* 2012). Cytoskeleton depolymerization drug treatment in this study was performed by incubating small leaf segments (3x3mm) in a solution containing latruculin b (25µM for 30-45min), Oryzalin (20 µM for 30-45min) or Amiprophos-methyl (APM; 50µM for 60-90min).

Transmission electron microscopy and immuno-gold labelling

Plant tissue was fixed by high-pressure freezing and freeze-substitution as described (Deeks *et al.,* 2012). The VAP27 anti-serum was used at 1:100 dilutions and detected by 5nm gold-conjugated anti-mouse IgG.

Gene Accession numbers

The Arabidopsis genome initiative locus tags for VAP27 genes are: At3g60600 (VAP27-1), At1g08820 (VAP27-2), At2g45140 (VAP27-3), At5g47180 (VAP27-4), At2g23820 (VAP27-5), At4g00170 (VAP27-6), At1g51270 (VAP27-7), At4g21450 (VAP27-8), At4g05060 (VAP27-9), At5g54110 (VAP27-10).

Results and Discussion

Phylogenetic analysis of Arabidopsis VAP27 proteins

Ten Arabidopsis VAP homologues (Fig. 1a) have been identified from a BLAST search using the Major Sperm Domain (MSD, Fig. 1b). Analysis based on full length protein sequences

show that VAP27 isoforms fall into three distinct clades. Although members within a clade can have different organizations of domains, all members of group two in particular lack a transmembrane domain and have the MSD located centrally rather than at the amino terminus. The majority of VAP27 isoforms show expression across a variety of tissues as shown by the genevestigator analysis (Fig. 1c). In addition to many other tissues, VAP27-1 and VAP27-4 show a peak of transcription in pollen. The tissues in which we find transcription of VAP27-5 & 7 are much more limited. VAP27-5 is confined to shoot, pollen and the stele. VAP27-7 is only found in the leaf although transcription is also seen in mesophyll and root primary cell culture.

Intracellular localization of VAP27 proteins in *N. benthamiana* leaf epidermal cells

Five of the ten VAP27 proteins have been used to make chimeric constructs with yellow fluorescent protein (YFP) at the C-terminus. These constructs were used for Argobacterium mediated transient transfection of *N. benthamiana* leaf epidermal cells in order to study their intracellular localization and behaviour. Our previous study showed that VAP27-1 is an ER integral membrane protein that also localised to EPCS (Wang *et al.,* 2014; Fig. 2a). A similar localisation pattern was observed for VAP27-3 (also known as PVA12, Saravanan *et al.,* 2009) and VAP27-4, representative members of clade 1 and clade 3 respectively. Both proteins localise to the ER network, confirmed by their co-localisation with CFP-HDEL, in addition to immobile punctate structures that we previously identified as EPCS (Fig. 2b-c; Movie S1). At the cell periphery, VAP27-1 puncta appeared to co-localise with the PM (stained with FM4-64, Fig. 2a, inset). Signals from the rest of the ER are very distinct from the PM (FM4-64 labelled, red). In contrast, two members from Clade 2 of the VAP27 family namely, YFP fusions of VAP27-8 and VAP27-10 (also known as AtMAMI, Galaud *et al.,* 1997), localise to the plasma membrane (Fig. 2d-f; Movie S2). They are very likely to be membrane peripheral proteins (as no transmembrane domain has been identified) recruited to the PM from a cytoplasmic pool. VAP27-8-YFP also labelled some immobile puncta (Fig. 2d) and is also found concentrated in the nucleolus (Fig. 2d, inset).

NET3C belongs to a plant specific family of actin binding proteins, the NET Family (Deeks *et al.,* 2012); it locates to the EPCS (Wang et al 2014). We have previously shown that VAP27-1 co-localises and interacts with NET3C at these sites (Wang *et al., 2014*). In this study, we

show that VAP27-3-YFP also co-localises with GFP-NET3C at EPCS when co-expressed in the transient expression system (Fig. 3a). We have confirmed the physical interaction between RFP-VAP27-3 and GFP-NET3C *in vivo* using FRET-FLIM microscopy (Fig. 3b-d). The fluorescent life time (LT) of GFP-NET3C (donor complex) was found to be 2.61 ± 0.05ns, which reduces significantly in the presence of RFP-VAP27-3 (LT=2.41 ± 0.05ns; p=7.63E-8), indicating that they interact in a complex. It should be noted that the life time of GFP-NET3C in the nucleus does not change as no VAP27-3 is present and this also acts as an internal control for this FRET-FLIM study (Fig. 3d). A second negative control was carried out using GFP-HDEL and RFP-HDEL; the life time of GFP in cells expressing both constructs was measured at 2.66 ± 0.03ns and this indicates that these two proteins which do localise to the same compartment do not interact and therefore do not undergo FRET (Fig. 3c).

Localisation of VAP27-1 in Arabidopsis

In order to assess the level of translational expression of VAP27-1 and VAP27-3, each gene was ligated in frame with GUS at the 3' end of each open reading frame. Expression in Arabidopsis revealed that both proteins are expressed ubiquitously (Fig. 4a-b), similar to their predicted transcriptional expression profiles (Fig. 1 c). Arabidopsis leaf epidermal cells were then used for further immuno-labelling studies.

A polyclonal antibody raised against VAP27-1 in mice detects a single band on a western blot of a total protein extract from Arabidopsis seedlings at a molecular weight similar to that for VAP27-1 (Fig. 4c). This antibody is specific to VAP27-1 when compared to its cross reactivity to VAP27-3 proteins, which have high overall sequence similarity (Fig. 4d). Cotyledons from a stable Arabidopsis line expressing VAP27-1-YFP were high pressure frozen and freeze-substituted for TEM and immuno-gold studies. The area of association (marked in red) between the ER and PM appears much enhanced by the expression of VAP27-1. Gaps between the ER and PM are almost undetectable (Fig. 4e-f). Gold labelled VAP27-1 is found throughout the ER network as well as at the EPCS (arrow, Fig. 4g).

Immunofluorescence studies using Arabidopsis leaf epidermal cells identifies the endogenous VAP27-1 on the ER network (which is stained by a BIP2 antibody) as well as some ER associated puncta that are distinct from the BIP2 labelled ER (Fig. 4h). The EPCS labelling of endogenous VAP27-1 in Arabidopsis is not as pronounced as the VAP27-1-YFP in

the tobacco transient expression system and this is likely to be because of the amount of protein that is present with more VAP-27-1-YFP being available in the transiently expressing cells. VAP27-1 signal is found at the same position as the BIP2 signal on the ER membrane. In contrast, VAP27-1 and BIP2 are only partially co-localized at the putative EPCS (Fig. S1). This makes sense because VAP27s (like yeast Scs2) are actively recruited to the EPCS, while other ER localised proteins are not.

Two strips of the same western blot of a 1D gel loaded with *N. benthamiana* leaf extract expressing VAP27-1-YFP were probed with 1.VAP27-1 antibody; 2.VAP27-1 antibody co-incubated with VAP-27 peptide immunogen. Incubating the VAP27-1 peptide immunogen with the VAP27-1 antibody abolished the ability of the antibody to detect a band on the western blot equivalent to VAP27-1-YFP indicating the antibody's specificity for VAP27-1 (Fig. 4j). Co-incubating the VAP27-1 peptide immunogen with the VAP27-1 antibody and using this mixture to stain Arabidopsis cells revealed no staining of the ER and EPCS *in planta* (Fig. 4i) further supporting the specificity of the VAP27-1 antibody used in this study. In summary, results from the immunocytochemistry are consistent with the live cell imaging data, confirming VAP27-1 as an ER network and EPCS localised protein in plants. We suggest that VAP proteins from clades 1 and 3, specifically VAP27-3 and VAP27-4, have a similar cellular location in Arabidopsis as their sequences are very similar to VAP27-1 (VAP27-3, 84%; VAP27-4, 57%) and their localisation in *N.benthamiana* is the same (Fig. 2a-c).

Stably transformed Arabidopsis expressing VAP27-1-GFP driven by its native promoter exhibit a similar subcellular localisation to that observed when using the same construct in the *N. benthamiana* transient expression system (Fig. 5a-c). Numerous ER-associated puncta are identified, reminiscent of the EPCS seen in leaf epidermal studies. However, these puncta are not seen in all cells. For example, in trichome development, EPCS labelling was only seen in mature trichomes (stage 6) and not found in the earlier developmental stages (stages 1-4) (Fig. 5 d-e). This is either because EPCS may not exist in this type of cell, or other proteins may be involved in EPCS formation. VAP27-1 labelled EPCS are found in close association with both the microtubule and actin cytoskeletons (Fig. 5g-i) in trichomes of the Arabidopsis stably transformed lines and in transiently expressing *N. benthamiana* leaf epidermal cells (Fig. S2a-f). In Arabidopsis trichomes for example, the percentage of EPCS that are associated with the actin cytoskeleton or with microtubules was found to be 81.2 ±

4.3% and 70.4 ± 14.3% respectively. A random association assessed by rotating the red channel (e.g. RFP-Lifeact) by 180^0 with respect to the green channel (VAP27-1-GFP) gave a percentage association of 40.1 ± 7.75%, which is significantly lower than the percentage association between EPCS and actin or microtubules indicating that their association with the cytoskeleton is a valid result.

VAP27-1 labelled EPCS are often located at the cross overs between F-actin and microtubules (Fig. S2d-f). This observation supports the observations that part of the ER sub-domain interacts with microtubules, forming so called C-MERs (cortical microtubule associated ER sites; Pena and Heinlein, 2013). However, these contact sites do not appear to be maintained by the cytoskeleton, as they still exist when either F-actin or microtubules are removed by drug treatments (Fig. S2g-i).

The dynamics of VAP27 at the ER/PM contact site (EPCS) is influenced by the cell wall.

A population of the VAP27-1-YFP labelled EPCS also associated with plasmodesmata as revealed by co-localisation of aniline blue staining of callose (Fig. 6a), suggesting that PDs may perform a similar function to the ER/PM contact site at the cell-cell border in terms of anchoring the peripheral ER. In this context, it is known that the desmotubule of plasmodesmata is comprised of highly constricted ER membrane (Wright *et al.,* 2007; Fitzgibbon *et al.,* 2010; Knox *et al.,* 2015) and as such a role of VAPs in anchoring the peripheral ER to the plasmodesmal channel is an attractive hypothesis.

Leaf epidermal cells expressing VAP27-1 were treated with mannitol to induce plasmolysis, designed to separate the plasma membrane from the cell wall (the PM in Fig. 6b-c is labelled with a fluorescence marker, PIP2-CFP). As a consequence, hechtian strands are found in the plasmolysed cells that link the cell wall and plasma membrane (Lang-Pauluzzi 2000; Fig. 6b-c). Surprisingly, most of the VAP27-1 labelled EPCS were found within or at the tips of hechtian strands (Fig. 6c-d). Thus, we suggest that the plant ER/PM complex must interact indirectly with the cell wall through some PM localised proteins, which holds them together during plasmolysis while the rest of the ER network is separated from the cell periphery (Fig. 6d).

Subsequently, protoplasts were isolated from VAP27-1-YFP transformed leaves to study the influence of the cell wall on the EPCS (Movies S3). After photobleaching, the recovery of VAP27-1 at the ER/PM contact site is calculated as 74.45 ± 15.9% (Fig. 6f-g). It is known that cell wall can be re-generated around protoplasts (Martiniere *et al.,* 2011). No cell wall staining is seen at 0 hours when the protoplasts were freshly prepared, whereas staining was seen at ca. 24 hours after isolation (Fig. 6e). When the cell wall reformed, the maximum recovery of VAP27-1 reduced to 57.48 ± 10.4%, significantly different from its recovery at 0 hours ($p < 0.001$). These differences in the percentage recoveries indicate that the immobile fraction of VAP27-1 within the photo-bleached region is greater when the cell wall has re-generated. This also indicates that the association between VAP27-1 labelled EPCS and the cell wall makes VAP27-1 largely immobile. However, the half time of recovery at both time points (0 and 24 hrs) does not change significantly ($p>0.2$) which indicates that the dynamics of VAP27-1 in the photobleached regions at 0 hours and ca. 24 hours are similar.

In conclusion, these results indicate that the cell wall affects the percentage recovery of the EPCS associated protein, VAP27-1. We suggest that this phenomenon is due to VAP27-1 interacting with a protein that both spans the plasma membrane and interacts with the cell wall and the EPCS at either terminus, or that VAP27-1 associates with a PM sub-domain whose mobility is constricted by the cell wall. Recently, the physical association of the cell wall with the plasma membrane has been implicated in the anchoring of many different proteins in the plasma membrane (Martiniere *et al.,* 2012). Both scenarios could affect protein dynamics at the plasma membrane and subsequently the EPCS (Fig. 6h).

Expression of VAP27-1 and NET3C induces PM associated ER cisternae

High level expression of constructs in the *N. benthamiana* transient system can be obtained by increasing the optical density of the Agrobacteria used for infiltration (Batoko *et al.,* 2000). When highly expressed, VAP27-1 interacts with NET3C and induces the formation of membrane cisternae, which are labelled by CFP-HDEL, suggesting that these cisternae are ER derived (Fig. 7a). EPCS labelling may still be seen in some parts of the cell (Fig. 7a, arrow), but the significant deformation of ER membrane makes these sites difficult to resolve. These ER derived membrane cisternae are closely attached to the PM, as seen by the close

association with FM4-64 fluorescence at the cell cortex (Fig. 7b-c; also compare with Fig. 1a, inset). Some filament-like structures in negative contrast can be observed within the membrane cisternae (Fig. 7d, arrow), and these co-localise with microtubules (labelled with the Kinesin Motor Domain fused to RFP; KMD-RFP). This microtubule related pattern in membranes has been previously described in several studies of plasma membrane integral proteins. This is likely due to the corralling of PM proteins by cortical microtubules (Martiniere and Runions, 2013). Not surprisingly, these negative images of microtubules disappear when microtubules are depolymerized by amiprophos-methyl (APM) treatment (Fig. 7e).

The enhanced association between the ER and PM membrane is only seen when both VAP27-1 and NET3C are present, and expression of VAP27-1 alone does not induce this phenomenon (Fig. 2a). This result suggests that only a small fraction of ER membrane can interact with PM associated NET3C to form the EPCS under native conditions where both VAP27 and NET3C expression are limiting. However, an excess level of both proteins appears to 'glue' the entire cortical ER system to the PM and induce this abnormal cellular phenotype (Fig. 7f).

Domain characterization of VAP27 using deletion mutants and live cell imaging

Three distinct functional domains are found in VAP27-1, namely, an N-terminal major sperm domain (MSD), a C-terminal transmembrane domain (TMD) and a coiled-coil domain (CCD). Domain deletion mutants of VAP27-1 were made and fused to YFP (Fig. 8a). VAP27-1ΔTMD was found to be cytosolic (Fig. 8e); VAP27-1ΔCCD-YFP is still ER localised but less puncta are observed than for full length VAP27 (Fig. 8c). The number of puncta was found to be 7.2 ± 3.1 per 30x30µm for VAP27-1ΔCCD compared to 31.4 ± 5.8 per 30x30µm for full length VAP27-1. VAP27-1ΔMSD-YFP forms numerous ER derived puncta, most of which are much more mobile than the full-length VAP27-1 puncta at ER/PM contact sites (Fig. 8d, Movie S4). Similar results were also obtained from a deletion study of another clade 1 VAP27, VAP27-3 (Fig. S3a-c). Little alteration of the ER network is seen in either the VAP27 full length (Fig. 2) or deletion mutant expressing cells (Fig. S3d-f). Therefore, the anchoring of the ER to the PM in plants may be complex and is likely to involve multiple proteins which includes the

association with NET3C (Wang *et al.,* 2014), and possibly synaptotagmins (Perez-Sancho *et al.,* 2015).

Protein dynamics within these puncta were studied using fluorescence recovery after photobleaching (FRAP; Fig. 8b). The maximum recovery of VAP27-1ΔCCD was found to be reduced (Rmax = 38.86 ± 18.5%) compared to full-length VAP27-1 (Rmax = 54.22 ± 18.2%; $p < 0.05$). VAP27-1ΔMSD showed almost no recovery over the same period (Fig. 8b). These results indicate that both MSD and CCD are important for the localization of VAP27 at the ER/PM contact site and most likely protein dynamics within the membrane, whereas, the TM domain determines the ER localisation of VAP27-1. Previously, we identified a functional motif on the major sperm domain required for the interaction between VAP27-1 and NET3C (Wang *et al.,* 2014). This result is consistent with an observation from the co-expression of NET3C with VAP27-1 deletion mutants in this study. That is, co-localisation of GFP-NET3C is only seen with VAP27-1ΔTMD which contains the intact major sperm domain (Fig. 8g), whereas, no co-localisation is seen between NET3C and VAP27-1ΔMSD (Fig. 8f).

Aberrant VAP27 expression effects plant development

We stably transformed Arabidopsis producing lines expressing VAP27-1-GFP or VAP27-3-GFP driven by their native promoters. As we have shown that the GFP constructs localise to the EPCS in a pattern also observed using anti-VAP27-1 *in planta*, and that from yeast studies chimeric Scs2-reporter proteins (homologue of VAP27) are functional (Loewen et al., 2007), then these constructs are likely to be functional in plants. These plants exhibit defects in pollen, seed and root development. The most notable defect is in root hair development where hairs appear branched (compare Fig. 9a with 9b, arrow). High magnification images of these abnormal root hairs are shown in Fig. 9i. This phenotype is also observed in VAP27-1 RNAi lines (Fig. 9c, arrow), which show a significant knock-down of endogenous VAP27-1 protein expression (Fig. 9f-g). A root hair phenotype is also seen in plants expressing VAP27-3-GFP as well as in VAP27-3 RNAi lines (Fig. 9d-e). The percentage of branched root hairs was calculated for each line and there were ca. 40% abnormal root hairs in the VAP27-GFP expressing lines, and ca. 15-20% in VAP27 RNAi lines (Fig. 9h). These observations are consistent in more than three independent transformed lines. It is interesting that a similar phenomenon is seen in either VAP27 gain of function and loss of

function studies. These data suggest that tight control of VAP27 expression is essential. A similar phenomenon is observed when the actin regulating protein, Actin Depolymerising Factor, is both over-expressed and knocked down (Dong *et al.,* 2001).

In the VAP27-1 expressing lines, both the ER and actin networks in the branched root hair are significantly different from those in the wild type (Fig. 9j-k). VAP27-1 labelled ER membrane aggregates formed at the point where the root hairs branch and the actin network appears disorganised in this zone (Fig. 9k). Root hair phenotypes have been observed previously when certain ER or F-actin regulating proteins are disrupted (Deeks *et al.,* 2007; Guimil and Dunand, 2007).

In conclusion, the VAP27 protein family has been identified and representative candidates selected for further functional characterization. Proteins from clade 1 and 3 localised to the ER network as well as the ER/PM contact sites, whereas members of clade 2 are found at the PM. The function of the different domains have been characterised using VAP27-1 and 3 as examples. We have demonstrated that the major sperm domain and coiled coil domain are required for protein-protein interaction and that the transmembrane domain is required for intracellular localization. Pleiotropic defects were seen in plants expressing VAP27-GFP and also in VAP27 RNAi lines, suggesting that they are essential for normal plant development. Our results also suggest an indirect association between ER/PM contact sites and the cell wall, likely to be mediated through interaction with PM associated proteins.

Acknowledgments This work was supported by a BBSRC grant (BB/G006334/1) to P.J.H and a Leverhulme Trust grant (F/00382/G) to CH.

Author Contribution: P.W. and P.J.H. planned and designed the research. P.W. performed the research, and together with P.J.H and C.H wrote the manuscript. C.R., T.J.H. and I.S. contribute to data analysis.

Total word: 4749

Reference

Barajas D, Xu K, de Castro Martin IF, Sasvari Z, Brandizzi F, Risco C, Nagy PD. 2014. Co-Opted Oxysterol-Binding Orp and Vap Proteins Channel Sterols to RNA Virus Replication Sites Via Membrane Contact Sites. *PLoS Pathog* **10**(10): e1004388.

Batoko H, Zheng HQ, Hawes C, Moore I. 2000. A Rab1 GTPase Is Required for Transport between the Endoplasmic Reticulum and Golgi Apparatus and for Normal Golgi Movement in Plants. *Plant Cell* **12**(11): 2201-2218.

Boevink P, Oparka K, Santa Cruz S, Martin B, Betteridge A, Hawes C. 1998. Stacks on Tracks: The Plant Golgi Apparatus Traffics on an Actin/ER Network. *Plant Journal* **15**(3): 441-447.

Carrasco S, Meyer T. 2011. STIM Proteins and the Endoplasmic Reticulum-Plasma Membrane Junctions. *Annual Review of Biochemistry* **80**: 973-1000.

daSilva LL, Snapp EL, Denecke J, Lippincott-Schwartz J, Hawes C, Brandizzi F. 2004. Endoplasmic Reticulum Export Sites and Golgi Bodies Behave as Single Mobile Secretory Units in Plant Cells. *Plant Cell* **16**(7): 1753-1771.

Deeks MJ, Calcutt JR, Ingle EK, Hawkins TJ, Chapman S, Richardson AC, Mentlak DA, Dixon MR, Cartwright F, Smertenko AP, Oparka K, Hussey PJ. 2012. A Superfamily of Actin-Binding Proteins at the Actin-Membrane Nexus of Higher Plants. *Current Biology* **22**(17): 1595-1600.

Deeks MJ, Rodrigues C, Dimmock S, Ketelaar T, Maciver SK, Malho R, Hussey PJ. 2007. Arabidopsis Cap1 - a Key Regulator of Actin Organisation and Development. *Journal of Cell Science* **120**(Pt 15): 2609-2618.

Dingsdale H, Okeke E, Awais M, Haynes L, Criddle DN, Sutton R, Tepikin AV. 2013. Saltatory Formation, Sliding and Dissolution of ER-PM Junctions in Migrating Cancer Cells. *Biochemical Journal* **451**(1): 25-32.

Dong CH, Xia GX, Hong Y, Ramachandran S, Kost B, Chua NH. 2001. ADF Proteins Are Involved in the Control of Flowering and Regulate F-Actin Organization, Cell Expansion, and Organ Growth in Arabidopsis. *Plant Cell* **13**(6): 1333-1346.

Fitzgibbon J, Bell K, King E, Oparka K. 2010. Super-Resolution Imaging of Plasmodesmata Using Three-Dimensional Structured Illumination Microscopy. *Plant Physiol* **153**(4): 1453-1463.

Guimil S, Dunand C. 2007. Cell Growth and Differentiation in Arabidopsis Epidermal Cells. *Journal of Experimental Botany* **58**(14): 3829-3840.

Hawes C, Kiviniemi P, Kriechbaumer V. 2014. The Endoplasmic Reticulum: A Dynamic and Well-Connected Organelle. *Journal of Integrative Plant Biology* **57**(1): 50-62.

Hawes C, Osterrieder A, Hummel E, Sparkes I. 2008. The Plant ER-Golgi Interface. *Traffic* **9**(10): 1571-1580.

Hawkins TJ, Deeks MJ, Wang P, Hussey PJ. 2014. The Evolution of the Actin Binding Net Superfamily. *Front Plant Sci* **5**: 254.

Helaers R, Milinkovitch MC. 2010. Metapiga V2.0: Maximum Likelihood Large Phylogeny Estimation Using the Metapopulation Genetic Algorithm and Other Stochastic Heuristics. *BMC Bioinformatics* **11**: 379.

Hepler PK, Palevitz BA, Lancelle SA, Mccauley MM, Lichtschidl I. 1990. Cortical endoplasmic reticulum in plants. *J Cell Sci* **96**:355-373.

Hilson P, Allemeersch J, Altmann T, Aubourg S, Avon A, Beynon J, Bhalerao RP, Bitton F, Caboche M, Cannoot B, Chardakov V, Cognet-Holliger C, Colot V, Crowe M, Darimont C, Durinck S, Eickhoff H, de Longevialle AF, Farmer EE, Grant M, Kuiper MT, Lehrach H, Leon C, Leyva A, Lundeberg J, Lurin C, Moreau Y, Nietfeld W, Paz-Ares J, Reymond P, Rouze P, Sandberg G, Segura MD, Serizet C, Tabrett A, Taconnat L, Thareau V, Van Hummelen P, Vercruysse S, Vuylsteke M, Weingartner M, Weisbeek PJ, Wirta V, Wittink FR, Zabeau M, Small I. 2004. Versatile Gene-Specific Sequence Tags for Arabidopsis Functional Genomics: Transcript Profiling and Reverse Genetics Applications. *Genome Research* **14**(10B): 2176-2189.

Hunter S, Jones P, Mitchell A, Apweiler R, Attwood TK, Bateman A, Bernard T, Binns D, Bork P, Burge S, de Castro E, Coggill P, Corbett M, Das U, Daugherty L, Duquenne L, Finn RD, Fraser M, Gough J, Haft D, Hulo N, Kahn D, Kelly E, Letunic I, Lonsdale D, Lopez R, Madera M, Maslen J, McAnulla C, McDowall J, McMenamin C, Mi H, Mutowo-Muellenet P, Mulder N, Natale D, Orengo C, Pesseat S, Punta M, Quinn AF, Rivoire C, Sangrador-Vegas A, Selengut JD, Sigrist CJ, Scheremetjew M, Tate J, Thimmajanarthanan M, Thomas PD, Wu CH, Yeats C, Yong SY. 2011. Interpro in 2011: New Developments in the Family and Domain Prediction Database. *Nucleic Acids Research* **40**(Database issue): D306-312.

Ketelaar T, Allwood EG, Anthony R, Voigt B, Menzel D,Hussey PJ. 2004. The Actin-Interacting Protein Aip1 Is Essential for Actin Organization and Plant Development. *Current Biology* **14**(2): 145-149.

Knox K, Wang P, Kriechbaumer V, Tilsner J, Frigerio L, Sparkes I, Hawes C, Oparka K. 2015. Putting the Squeeze on Plasmodesmata: A Role for Reticulons in Primary Plasmodesmata Formation. *Plant Physiol* **168**(4): 1563-1572.

Galaud JP, Laval V, Carriere M, Barre A, Canut H, Rouge P, Pont-Lezica R. 1997. Osmotic Stress Activated Expression of an Arabidopsis Plasma Membrane-Associated Protein: Sequence and Predicted Secondary Structure. *Biochimica et Biophysica Acta* **1341**(1): 79-86.

Lang-Pauluzzi I. 2000. The Behaviour of the Plasma Membrane During Plasmolysis: A Study by UV Microscopy. *J Microsc* **198**(Pt 3): 188-198.

Larkin MA, Blackshields G, Brown NP, Chenna R, McGettigan PA, McWilliam H, Valentin F, Wallace IM, Wilm A, Lopez R, Thompson JD, Gibson TJ, Higgins DG. 2007. Clustal W and Clustal X Version 2.0. *Bioinformatics* **23**(21): 2947-2948.

Laurent F, Labesse G, de Wit P. 2000. Molecular Cloning and Partial Characterization of a Plant Vap33 Homologue with a Major Sperm Protein Domain. *Biochemical and Biophysical Research Communications* **270**(1): 286-292.

Lemmon AR, Milinkovitch MC. 2002. The Metapopulation Genetic Algorithm: An Efficient Solution for the Problem of Large Phylogeny Estimation. *Proceedings of the National Academy of Sciences of the United States of America* **99**(16): 10516-10521.

Levy A, Zheng JY, Lazarowitz SG. 2015. Synaptotagmin Syta Forms ER-Plasma Membrane Junctions That Are Recruited to Plasmodesmata for Plant Virus Movement. *Current Biology* **25**(15): 2018-2025.

Loewen CJ, Levine TP. 2005. A Highly Conserved Binding Site in Vesicle-Associated Membrane Protein-Associated Protein (VAP) for the FFAT Motif of Lipid-Binding Proteins. *Journal of Biological Chemistry* **280**(14): 14097-14104.

Loewen CJ, Young BP, Tavassoli S, Levine TP. 2007. Inheritance of Cortical ER in Yeast Is Required for Normal Septin Organization. *Journal of Cell Biology* **179**(3): 467-483.

Lupas A, Van Dyke M, Stock J. 1991. Predicting Coiled Coils from Protein Sequences. *Science* **252**(5009): 1162-1164.

Manford AG, Stefan CJ, Yuan HL, Macgurn JA, Emr SD. 2012. ER-to-Plasma Membrane Tethering Proteins Regulate Cell Signaling and ER Morphology. *Developmental Cell* **23**(6): 1129-1140.

Martiniere A, Gayral P, Hawes C, Runions J. 2011. Building Bridges: Formin1 of Arabidopsis Forms a Connection between the Cell Wall and the Actin Cytoskeleton. *Plant Journal* **66**(2): 354-365.

Martiniere A, Lavagi I, Nageswaran G, Rolfe DJ, Maneta-Peyret L, Luu DT, Botchway SW, Webb SE, Mongrand S, Maurel C, Martin-Fernandez ML, Kleine-Vehn J, Friml J, Moreau PRunions J. 2012. Cell Wall Constrains Lateral Diffusion of Plant Plasma-Membrane Proteins. *Proceedings of the National Academy of Sciences of the United States of America* **109**(31): 12805-12810.

Martiniere A, Runions J. 2013. Protein Diffusion in Plant Cell Plasma Membranes: The Cell-Wall Corral. *Front Plant Sci* **4**: 515.

Mehrshahi P, Johnny C, DellaPenna D. 2014. Redefining the Metabolic Continuity of Chloroplasts and ER. *Trends in Plant Science* **19**(8): 501-507.

Pena EJ, Heinlein M. 2013. Cortical Microtubule-Associated ER Sites: Organization Centers of Cell Polarity and Communication. *Current Opinion in Plant Biology* **16**(6): 764-773.

Petersen NH, Joensen J, McKinney LV, Brodersen P, Petersen M, Hofius DMundy J. 2009. Identification of Proteins Interacting with Arabidopsis ACD11. *Journal of Plant Physiology* **166**(6): 661-666.

Perez-Sancho J, Vanneste S, Lee E, McFarlane HE, Esteban Del Valle A, Valpuesta V, Friml J, Botella MARosado A. 2015. The Arabidopsis Synaptotagmin1 Is Enriched in Endoplasmic Reticulum-Plasma Membrane Contact Sites and Confers Cellular Resistance to Mechanical Stresses. *Plant Physiol* **168**(1): 132-143.

Saravanan RS, Slabaugh E, Singh VR, Lapidus LJ, Haas T, Brandizzi F. 2009. The Targeting of the Oxysterol-Binding Protein Orp3a to the Endoplasmic Reticulum Relies on the Plant Vap33 Homolog Pva12. *Plant Journal* **58**(5): 817-830.

Schultz J, Milpetz F, Bork P, Ponting CP. 1998. Smart, a Simple Modular Architecture Research Tool: Identification of Signaling Domains. *Proceedings of the National Academy of Sciences of the United States of America* **95**(11): 5857-5864.

Skehel PA, Martin KC, Kandel ER, Bartsch D. 1995. A Vamp-Binding Protein from Aplysia Required for Neurotransmitter Release. *Science* **269**(5230): 1580-1583.

Soussan L, Burakov D, Daniels MP, Toister-Achituv M, Porat A, Yarden Y, Elazar Z. 1999. ERG30, a VAP-33-Related Protein, Functions in Protein Transport Mediated by COPI Vesicles. *Journal of Cell Biology* **146**(2): 301-311.

Sparkes IA, Ketelaar T, de Ruijter NC, Hawes C. 2009a. Grab a Golgi: Laser Trapping of Golgi Bodies Reveals in Vivo Interactions with the Endoplasmic Reticulum. *Traffic* **10**(5): 567-571.

Sparkes I, Runions J, Hawes C, Griffing L. 2009b. Movement and Remodeling of the Endoplasmic Reticulum in Nondividing Cells of Tobacco Leaves. Plant Cell **21**(12): 3937-3949.

Stefano G, Hawes C, Brandizzi F. 2014. ER - the Key to the Highway. *Current Opinion in Plant Biology* **22C**: 30-38.

Stefan CJ, Manford AG, Baird D, Yamada-Hanff J, Mao Y, Emr SD. 2011. Osh Proteins Regulate Phosphoinositide Metabolism at ER-Plasma Membrane Contact Sites. *Cell* **144**(3): 389-401.

Sonnhammer EL, von Heijne G, Krogh A. 1998. A Hidden Markov Model for Predicting Transmembrane Helices in Protein Sequences. *Proc Int Conf Intell Syst Mol Biol* **6**: 175-182.

Varnai P, Toth B, Toth DJ, Hunyady L, Balla T. 2007. Visualization and Manipulation of Plasma Membrane-Endoplasmic Reticulum Contact Sites Indicates the Presence of Additional Molecular Components within the Stim1-Orai1 Complex. *Journal of Biological Chemistry* **282**(40): 29678-29690.

Wang P, Hawkins TJ, Richardson C, Cummins I, Deeks MJ, Sparkes I, Hawes C, Hussey PJ. 2014. The Plant Cytoskeleton, NET3C, and VAP27 Mediate the Link between the Plasma Membrane and Endoplasmic Reticulum. *Current Biology* **24**(12): 1397-1405.

Wang P, Hummel E, Osterrieder A, Meyer AJ, Frigerio L, Sparkes I, Hawes C. 2011. KMS1 and KMS2, Two Plant Endoplasmic Reticulum Proteins Involved in the Early Secretory Pathway. *Plant Journal* **66**(4): 613-628.

Weir ML, Xie H, Klip A, Trimble WS. 2001. VAP-A Binds Promiscuously to Both v- and tSNAREs. Biochemical and Biophysical Research Communications 286(3): 616-621.

Weir ML, Klip A, Trimble WS. 1998. Identification of a Human Homologue of the Vesicle-Associated Membrane Protein (Vamp)-Associated Protein of 33 Kda (Vap-33): A Broadly Expressed Protein That Binds to Vamp. *Biochemical Journal* **333 (Pt 2)**: 247-251.

Wesley SV, Helliwell CA, Smith NA, Wang MB, Rouse DT, Liu Q, Gooding PS, Singh SP, Abbott D, Stoutjesdijk PA, Robinson SP, Gleave AP, Green AGWaterhouse PM. 2001. Construct Design for Efficient, Effective and High-Throughput Gene Silencing in Plants. *Plant Journal* **27**(6): 581-590.

Wright KM, Wood NT, Roberts AG, Chapman S, Boevink P, Mackenzie KM, Oparka KJ. 2007. Targeting of TMV Movement Protein to Plasmodesmata Requires the Actin/ER Network: Evidence from FRAP. *Traffic* **8**(1): 21-31.

Zimmermann P, Hirsch-Hoffmann M, Hennig L, Gruissem W. 2004. Genevestigator. Arabidopsis Microarray Database and Analysis Toolbox. *Plant Physiol* **136**(1): 2621-2632.

Zhang C, Mallery EL, Szymanski DB. 2013. Arp2/3 Localization in Arabidopsis Leaf Pavement Cells: A Diversity of Intracellular Pools and Cytoskeletal Interactions. *Front Plant Sci* **4**: 238.

Figure legends

Figure 1. Phylogenetic analysis of the Arabidopsis VAP family.

(a) Phylogenetic tree of VAP27 isoforms (bootstrap values shown at nodes) with domain composition schematics for each protein. Red box = Major Sperm Domain, Blue box = Coiled Coil domain, Orange box = Transmembrane domain & green box = Toll interleukin 1 resistance domain. VAP27 protein sequences fall into 3 distinct clades. **(b)** VAP27 Major Sperm Domain (MSD) protein sequence alignment. ClustalX default residue colouring scheme based on physiochemical properties. **(c)** Heatmap of VAP family transcript level profiles, adapted from publicly available DNA microarray data and visualised with gene investigator. VAP27-2 is not included here as these are absent from the 22K Arabidopsis genechip.

Figure 2. Intracellular localization of VAP27 proteins using fluorescence protein fusions and transient expression in *N.benthamiana* leaf epidermal cells.

(a-c) Arabidopsis VAP27-1-YFP, VAP27-3-YFP and VAP27-4-YFP (red) localises to the ER (CFP-HDEL, green) as well as multiple immobile punctate structures that are the ER/PM contact sites. These ER/PM contact sites are structurally distinct from the ER network and do not co-localize with the CFP-HDEL signal. VAP27-1 labelled ER/PM contact sites (green) co-localise with FM4-64 (red) at the cell cortex, indicating that they are associated with the PM (a, inset). **(d-e)** VAP27-8 and VAP27-10 belong to clade 2 of the VAP family and they both localise to the PM. VAP27-8-YFP (red) labels some PM associated puncta that are not ER associated. VAP27-8-YFP is also found to be concentrated at the nucleolus (inset). **(f)** FM4-64 (red) labels the plasma membrane, VAP27-8-YFP (green) co-localises with FM4-64 confirming its PM localization (scale bar = 10µm).

Figure 3. NET3C interacts with VAP27-3 at the ER/PM contact sites in *N.benthamiana* leaf epidermal cells.

(a) VAP27-3-YFP (red) co-localises with GFP-NET3C at the ER/PM contact site. **(b-c)** Protein interactions between VAP27-3 and NET3C were analysed using FRET-FLIM. The life time (LT) of GFP-NET3C is 2.61 ± 0.05ns on its own, and the life time for GFP-HDEL in the presence of RFP-HDEL is 2.66 ± 0.03ns. **(d)** When GFP-NET3C is co-expressed with RFP-VAP27-3, the LT of GFP reduced to 2.41 ± 0.05ns, indicating a protein-protein interaction (scale bar = 10µm).

Figure 4. Analysis of the expression profile of VAP27-1 and 3 using GUS staining in Arabidopsis stably transformed lines and the identification of ER/PM contact sites.

(a-b) The expression pattern of VAP27-1 and VAP27-3 is confirmed using GUS reporter gene. Both proteins are expressed ubiquitously in Arabidopsis. GUS staining of cotyledons (1), root (2), trichomes (3-4), pollen and pollen tube (5) and embryo (6) are shown. **(c)** Western blot of total Arabidopsis seedling protein extract probed with a polyclonal VAP27-1 antibody showing a clear band at 27 kDa. **(d)** Western blot of protein extracts from *N.Benth* expressing VAP27-1-YFP and VAP27-3-YFP. Equal total proteins were load on each lane (amido black), only the VAP27-1 is strongly recognized by the VAP27-1 antibody. **(e-f)** TEM images of Arabidopsis leaf cells expressing VAP27-1-YFP (35s promoter driven). Close association between the ER and PM is observed at the ultra-structural level. ER membrane is completely attached to the PM with no space in between (highlighted). **(g)** Immuno-gold labelling of sections from stable VAP27-1-YFP Arabidopsis cotyledons using VAP27 antibodies. Gold particles are found throughout the ER membrane as well as at the ER/PM contact sites (arrowhead), which is consistent with the results obtained from TEM and confocal studies. **(h)** Immuno-fluorescence of Arabidopsis leaf epidermal cells with VAP27-1 (TRITC, red) and BIP2 (FITC, green) antibodies. Endogenous VAP27-1 localises to the ER as well as some ER associated puncta which are distinct from ER membrane labelled by BIP2. **(i)** Immuno-fluorescence was performed as in (h) but in the present of VAP27-1 peptide immunogen, the VAP27-1 labelling (red) seen previously was abolished with no effect on the BIP2 labelling of the ER (green). **(j)** Western blots of the same 1D gel of Leaf extracts expressing VAP27-1-YFP using, 1, VAP-27-1 antibody; 2, VAP-27-1 antibody coincubated with the VAP27-1 peptide immunogen. Note that no band at the same molecular weight as VAP27-1-YFP was detected in lane 2 (scale bar = 10µm for confocal; 500nm for TEM).

Figure 5. VAP27-1-GFP expression in stably transformed Arabidopsis lines.

(a-c) In Arabidopsis cotyledon, shoot meristem and root elongating cells, VAP27-1-GFP (driven by its native promoter) localises to the ER network and ER/PM contact sites, which is similar to the results when the construct is expressed in the transient *N.benthamiana* expression system. **(d-f)** However, no EPCS labelling was seen in trichome at early developmental stages (stage 1-4). EPCS was only seen in mature trichome (stage 5-6). **(g-i)** In mature trichomes, both actin and microtubule cytoskeleton were found closely associated with EPCS labelled by VAP27-1-GFP (scale bar = 10µm).

Figure 6. VAP27 labelled ER/PM contact sites were found within the Hechtian strands of *N. benthamiana* leaf epidermal cells, and their mobility is influenced by the cell wall.

(a) Some VAP27 labelled ER/PM contact sites co-localise with plasmodesmata (green, labelled with aniline blue), however the number of PD is much less than the number of ER/PM contact sites. (**b**) An example of plasmolysis and formation of hechtian strands induced by mannitol treatment. PM is labelled by PIP2-CFP. **(c)** VAP27-1 labelled ER/PM contact sites (red) were found within the hechtian strands (green) after plasmolysis, most of which were found at the tips of those strands indicating they are connected to the cell wall**.** **(d)** Diagrammatic illustration of the observations during plasmolysis. **(e)** Protoplasts were isolated from leaves expressing VAP27-1-YFP (green). No cell wall staining was seen using freshly prepared cells. However, the cell wall starts to re-build around the protoplasts and this was stained strongly (blue) 24 hours after isolation. **(f)** Dynamics of VAP27 at the ER/PM contact sites of protoplasts using FRAP. Enhanced mobility of VAP27 (Rmax=74.45 ± 15.9%) is evident when the cell wall is removed. However, VAP27 at the ER/PM contact sites becomes less mobile (Rmax=57.48 ± 10.4%) after 24 hours as the cell wall recovers. **(g)** Representative images of the FRAP experiment of VAP27; images from pre-bleach, bleach and 80 seconds post-bleach are shown. **(h)** Diagrammatic illustration of two possibilities of how the cell wall could influence the mobility of VAP27, either through interaction with PM spanned proteins (i) or by associating with certain PM subdomains (ii) (scale bar = 10µm for confocal; 500nm for TEM).

Figure 7. Expression of NET3C and VAP27 change the ER morphology and enhance the association between ER and PM in transiently transformed *N. benthamiana* leaf epidermal cells.

(a) Pro-longed expression of VAP27-1-YFP (magenta), RFP-NET3C (red) and CFP-HDEL (green). Most of the tubular ER network is converted to ER cisternae; negatively labelled thick strips are seen going across the ER derived membrane. **(b-c)** VAP27/NET3C expression induced membrane cisternae were found very close to the PM (labelled by FM4-64, red). At the cell periphery, these membranes co-localise with FM4-64 indicating that the altered ER network is 'glued' to the PM**. (d-e)** Microtubules (RFP-KMD, red) co-align with the negatively labelled strips (arrow) which are induced by VAP27/NET3C expression, and these strips can be removed by treating with the microtubule depolymerisation drug, APM. **(f)** Diagrammatic illustration of the mechanism by which the ER network is attached to the PM when both VAP27 and NET3C are over-expressed. However, less ER/PM association will occur in the native condition as the expression of both VAP27 and NET3C are limited (scale bar = 10µm).

Figure 8. Localisation and dynamics of VAP27 domain deletion mutants in transiently transformed *N. benthamiana* leaf epidermal cells.

(a) Diagrammatic illustration of the fluorescent protein fusions of VAP27 or VAP27 deletion mutants used in this study. **(b)** Protein dynamics within the ER/PM contact site or punctate structures analysed using FRAP. The mobility of full length VAP27-1 is much greater (Rmax = 54.2 ± 18.2%) than the coiled-coil domain deletion mutants (Rmax = 38.9 ± 18.5%). The punctae induced by VAP27-1ΔMSD exhibited little recovery during the time course **(c)** VAP27-1 without the coil-coiled domain (ΔCCD) localises to the ER network. Punctate structures still formed at the ER nodules, and the morphology of the ER does not change significantly. (**d)** VAP27-1 without the major sperm domain (ΔMSD) forms ER associated protein aggregates, which are very mobile. **(e)** VAP27 without the transmembrane domain (ΔTMD) distributed to the cytoplasm. It did not localise to the PM, which indicates that the transmembrane domain is essential for ER targeting as well as for PM interaction. **(f)** Punctate structures labelled by VAP27-1ΔMSD-YFP (red) did not co-localise with GFP-NET3C (green), indicating that they are unlikely to be the ER/PM contact sites and that the major sperm domain is required for VAP27-NET3C interaction. **(g)** VAP27-1ΔTMD-YFP (red) is recruited from the cytoplasm to PM when co-expressed with NET3C (green; scale bar = 10μm).

Figure 9. The change in the level of expression of VAP27 in Arabidopsis leads to developmental defects in root hairs.

(a) Root hairs found within the differentiation zone of wild type Arabidopsis. **(b)** The root hairs from VAP27-1 expressing Arabidopsis lines exhibit an abnormal phenotype. They are much shorter and swollen compared to the wild type, and most are branched. **(c)** Brached root hairs were also seen in VAP27-1 RNAi lines (arrow), suggesting that either over- or under-expression of VAP27 affects root hair development. **(d-e)** The branched root hair phenotype is also observed in VAP27-3 expressing and VAP27-3 RNAi plants. **(f)** Western blot of VAP27-1 RNAi Arabidopsis (1-3) and wild type, the knock-down of VAP27-1 protein was confirmed in these RNAi lines. **(g)** Amido black staining suggested equal amount of proteins were loaded in all lanes (lower panel). **(h)** Statistical analysis of branched root hairs in VAP27-1 and 3 over-expression or knock-down lines. The percentage for each line is shown in the table. **(i)** Branched root hairs at high magnification, two root hairs were often seen bulged from one trichoblast cell. **(j)** The actin cytoskeleton (labelled by GFP-Lifact) in a wild type root hair cell, with fine filaments in the apical part and thick bundles at the base (3D maximum projection). **(k)** In the VAP27-1 expressing root hair cells, the ER and F-actin form aggregates, which affect its polarised growth. Instead of growing directionally, the root hair cell branched at the point where the membrane aggregates assemble (3D maximum projection; scale bar = 10μm).

.

Supplementary figure legends

Figure S1. Fluorescence signal distribution of VAP27-1-YFP on ER membrane.

Figure S2. The ER/PM contact sites in relation to the cytoskeleton.

Figure S3. VAP27 deletion mutants exhibit little effect on ER morphology

Table S1. List of primers used in this study.

Table S2. List of plasmids used in this study.

Supplementary movies

M**oviesS1,** Z-stack images of leaf cells transiently expressing VAP27-4-YFP, which localises to the ER network as well as the EPCS.

Movie S2, Z-stack images of leaf cells transiently expressing VAP27-8-YFP, which localises to the PM.

Movie S3, Protoplast expressing VAP27-1-YFP.

Movie S4, VAP27-1-YFPΔMSD (red) co-expressed with GFP-HDEL (green) in leaf epidermal cells. VAP27-1ΔMSD punctae are more mobile than they are when the full length protein is used

Figure 1

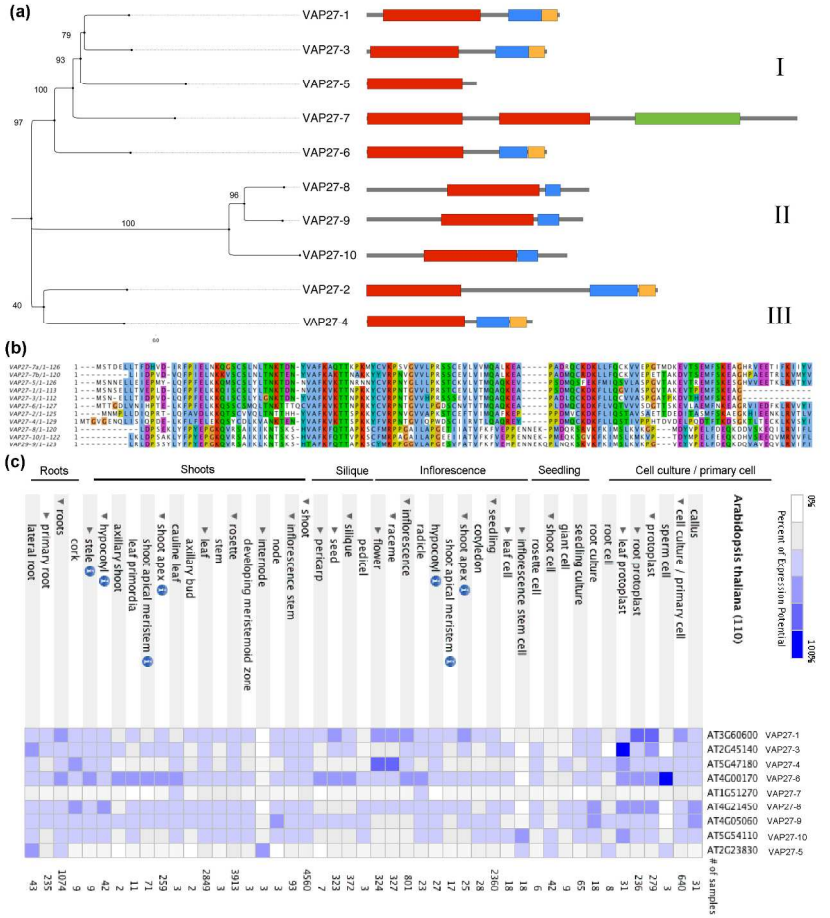

Figure 1. Phylogenetic analysis of the Arabidopsis VAP family.
(a) Phylogenetic tree of VAP27 isoforms (bootstrap values shown at nodes) with domain composition schematics for each protein. Red box = Major Sperm Domain, Blue box = Coiled Coil domain, Orange box = Transmembrane domain & green box = Toll interleukin 1 resistance domain. VAP27 protein sequences fall into 3 distinct clades. (b) VAP27 Major Sperm Domain (MSD) protein sequence alignment. ClustalX default residue colouring scheme based on physiochemical properties. (c) Heatmap of VAP family transcript level profiles, adapted from publicly available DNA microarray data and visualised with gene investigator. VAP27-2 is not included here as these are absent from the 22K Arabidopsis genechip.

209x297mm (300 x 300 DPI)

Figure 2

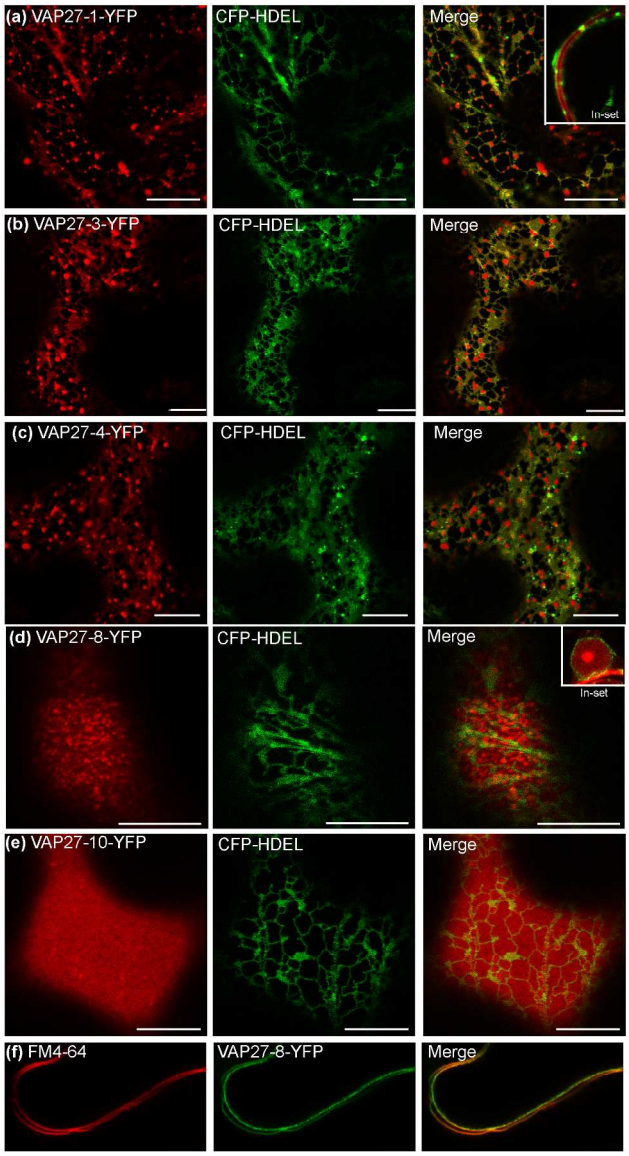

Figure 2. Intracellular localization of VAP27 proteins using fluorescence protein fusions and transient expression in N.benthamiana leaf epidermal cells.
(a-c) Arabidopsis VAP27-1-YFP, VAP27-3-YFP and VAP27-4-YFP (red) localises to the ER (CFP-HDEL, green) as well as multiple immobile punctate structures that are the ER/PM contact sites. These ER/PM contact sites are structurally distinct from the ER network and do not co-localize with the CFP-HDEL signal. VAP27-1 labelled ER/PM contact sites (green) co-localise with FM4-64 (red) at the cell cortex, indicating that they are associated with the PM (a, inset). (d-e) VAP27-8 and VAP27-10 belong to clade 2 of the VAP family and they both localise to the PM. VAP27-8-YFP (red) labels some PM associated puncta that are not ER associated. VAP27-8-YFP is also found to be concentrated at the nucleolus (inset). (f) FM4-64 (red) labels the plasma membrane, VAP27-8-YFP (green) co-localises with FM4-64 confirming its PM localization (scale bar = 10μm).

209x297mm (300 x 300 DPI)

Figure 3

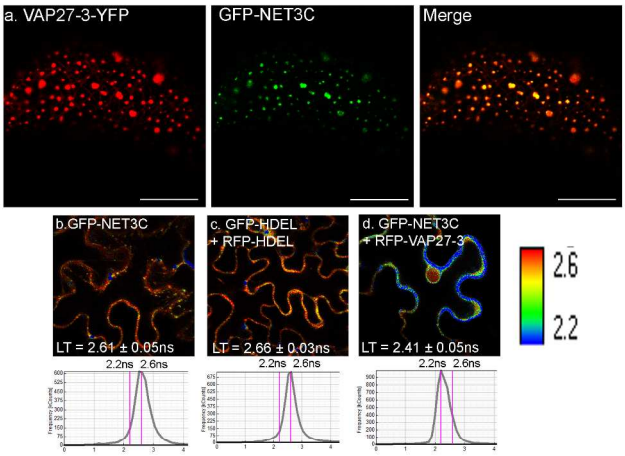

Figure 3. NET3C interacts with VAP27-3 at the ER/PM contact sites in N.benthamiana leaf epidermal cells. (a) VAP27-3-YFP (red) co-localises with GFP-NET3C at the ER/PM contact site. (b-c) Protein interactions between VAP27-3 and NET3C were analysed using FRET-FLIM. The life time (LT) of GFP-NET3C is 2.61 ± 0.05ns on its own, and the life time for GFP-HDEL in the presence of RFP-HDEL is 2.66 ± 0.03ns. When GFP-NET3C is co-expressed with RFP-VAP27-3, the LT of GFP reduced to 2.41 ± 0.05ns, indicating a protein-protein interaction (scale bar = 10μm).

209x297mm (300 x 300 DPI)

Figure 4

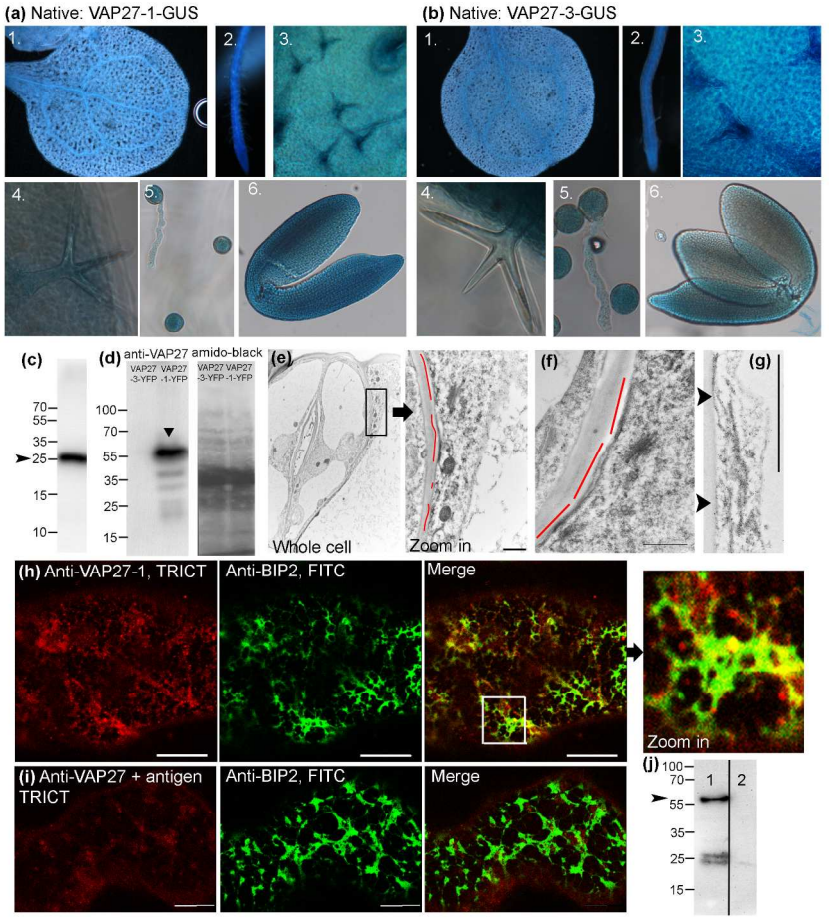

Figure 4. Analysis of the expression profile of VAP27-1 and 3 using GUS staining in Arabidopsis stably transformed lines and the identification of ER/PM contact sites.

(a-b) The expression pattern of VAP27-1 and VAP27-3 is confirmed using GUS reporter gene. Both proteins are expressed ubiquitously in Arabidopsis. GUS staining of cotyledons (1), root (2), trichomes (3-4), pollen and pollen tube (5) and embryo (6) are shown. (c) Western blot of total Arabidopsis seedling protein extract probed with a polyclonal VAP27-1 antibody showing a clear band at 27 kDa. (d) Western blot of protein extracts from N.Benth expressing VAP27-1-YFP and VAP27-3-YFP. Equal total proteins were load on each lane (amido black), only the VAP27-1 is strongly recognized by the VAP27-1 antibody. (e-f) TEM images of Arabidopsis leaf cells expressing VAP27-1-YFP (35s promoter driven). Close association between the ER and PM is observed at the ultra-structural level. ER membrane is completely attached to the PM with no space in between (highlighted). (g) Immuno-gold labelling of sections from stable VAP27-1-YFP Arabidopsis cotyledons using VAP27 antibodies. Gold particles are found throughout the ER membrane as well as at the ER/PM contact sites (arrowhead), which is consistent with the results obtained from TEM and confocal

studies. (h) Immuno-fluorescence of Arabidopsis leaf epidermal cells with VAP27-1 (TRITC, red) and BIP2 (FITC, green) antibodies. Endogenous VAP27-1 localises to the ER as well as some ER associated puncta which are distinct from ER membrane labelled by BIP2. (i) Immuno-fluorescence was performed as in (h) but in the present of VAP27-1 peptide immunogen, the VAP27-1 labelling (red) seen previously was abolished with no effect on the BIP2 labelling of the ER (green). (j) Western blots of the same 1D gel of Leaf extracts expressing VAP27-1-YFP using, 1, VAP-27-1 antibody; 2, VAP-27-1 antibody coincubated with the VAP27-1 peptide immunogen. Note that no band at the same molecular weight as VAP27-1-YFP was detected in lane 2 (scale bar = 10μm for confocal; 500nm for TEM).

209x297mm (300 x 300 DPI)

Figure 5

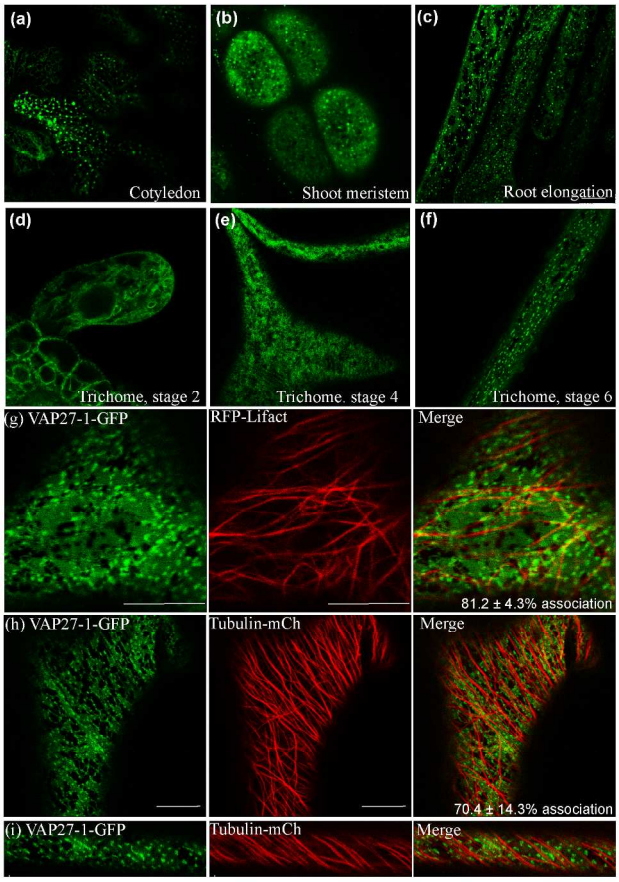

Figure 5. VAP27-1-GFP expression in stably transformed Arabidopsis lines. \r\n(a-c) In Arabidopsis cotyledon, shoot meristem and root elongating cells, VAP27-1-GFP (driven by its native promoter) localises to the ER network and ER/PM contact sites, which is similar to the results when the construct is expressed in the transient N.benthamiana expression system. (d-f) However, no EPCS labelling was seen in trichome at early developmental stages (stage 1-4). EPCS was only seen in mature trichome (stage 5-6). (g-i) In mature trichomes, both actin and microtubule cytoskeleton were found closely associated with EPCS labelled by VAP27-1-GFP. \r\n
209x297mm (300 x 300 DPI)

Figure 6

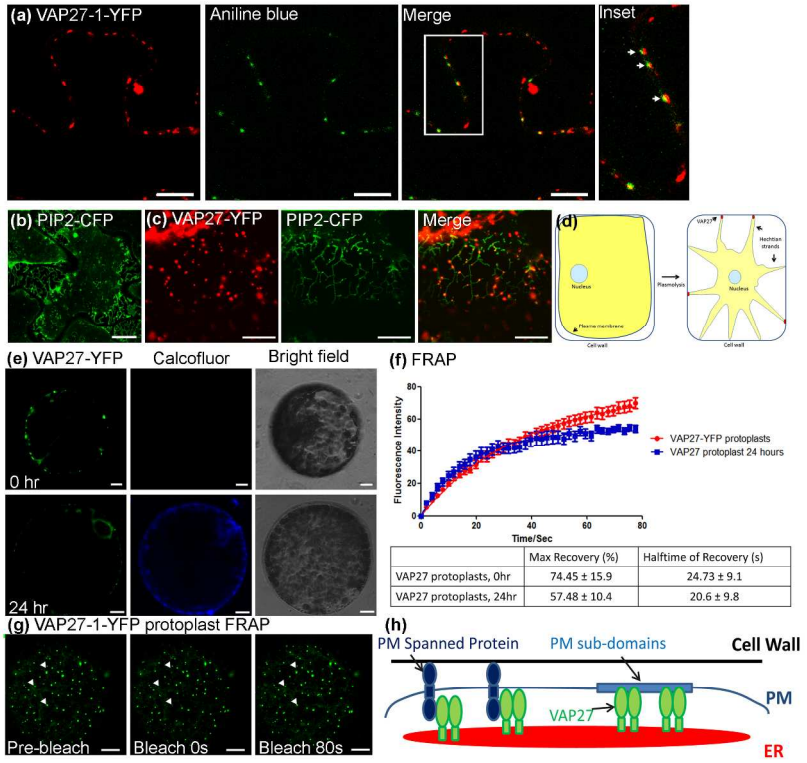

	Max Recovery (%)	Halftime of Recovery (s)
VAP27 protoplasts, 0hr	74.45 ± 15.9	24.73 ± 9.1
VAP27 protoplasts, 24hr	57.48 ± 10.4	20.6 ± 9.8

Figure 6. VAP27 labelled ER/PM contact sites were found within the Hechtian strands of N. benthamiana leaf epidermal cells, and their mobility is influenced by the cell wall.
(a) Some VAP27 labelled ER/PM contact sites co-localise with plasmodesmata (green, labelled with aniline blue), however the number of PD is much less than the number of ER/PM contact sites. (b) An example of plasmolysis and formation of hechtian strands induced by mannitol treatment. PM is labelled by PIP2-CFP. (c) VAP27-1 labelled ER/PM contact sites (red) were found within the hechtian strands (green) after plasmolysis, most of which were found at the tips of those strands indicating they are connected to the cell wall. (d) Diagrammatic illustration of the observations during plasmolysis. (e) Protoplasts were isolated from leaves expressing VAP27-1-YFP (green). No cell wall staining was seen using freshly prepared cells. However, the cell wall starts to re-build around the protoplasts and this was stained strongly (blue) 24 hours after isolation. (f) Dynamics of VAP27 at the ER/PM contact sites of protoplasts using FRAP. Enhanced mobility of VAP27 (Rmax=74.45 ± 15.9%) is evident when the cell wall is removed. However, VAP27 at the ER/PM contact sites becomes less mobile (Rmax=57.48 ± 10.4%) after 24 hours as the cell wall recovers.

(g) Representative images of the FRAP experiment of VAP27; images from pre-bleach, bleach and 80 seconds post-bleach are shown. (h) Diagrammatic illustration of two possibilities of how the cell wall could influence the mobility of VAP27, either through interaction with PM spanned proteins (i) or by associating with certain PM subdomains (ii) (scale bar = 10μm for confocal; 500nm for TEM).

209x297mm (300 x 300 DPI)

Figure 7

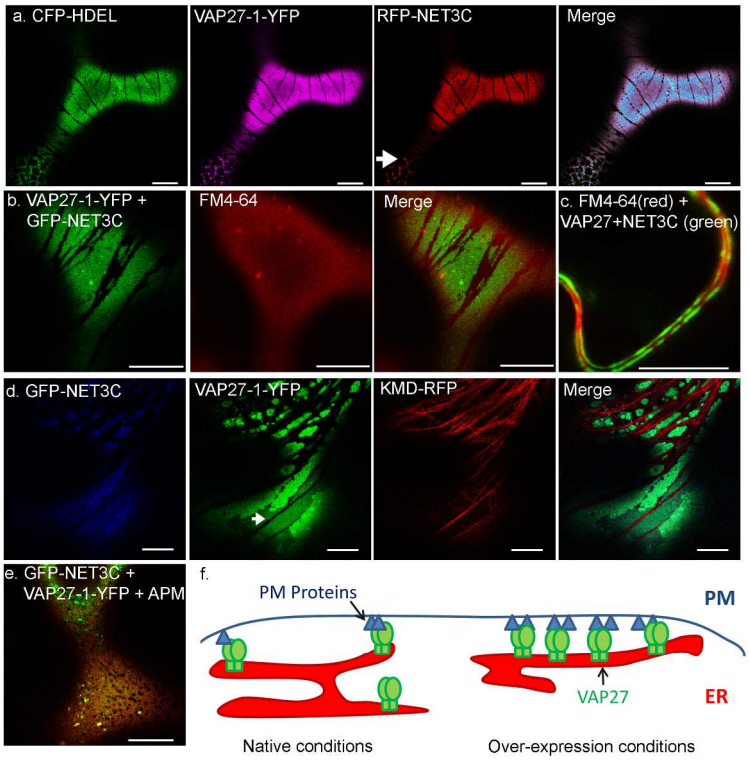

Figure 7. Expression of NET3C and VAP27 change the ER morphology and enhance the association between ER and PM in transiently transformed N. benthamiana leaf epidermal cells.

(a) Pro-longed expression of VAP27-1-YFP (magenta), RFP-NET3C (red) and CFP-HDEL (green). Most of the tubular ER network is converted to ER cisternae; negatively labelled thick strips are seen going across the ER derived membrane. (b-c) VAP27/NET3C expression induced membrane cisternae were found very close to the PM (labelled by FM4-64, red). At the cell periphery, these membranes co-localise with FM4-64 indicating that the altered ER network is 'glued' to the PM. (d-e) Microtubules (RFP-KMD, red) co-align with the negatively labelled strips (arrow) which are induced by VAP27/NET3C expression, and these strips can be removed by treating with the microtubule depolymerisation drug, APM. (f) Diagrammatic illustration of the mechanism by which the ER network is attached to the PM when both VAP27 and NET3C are over-expressed. However, less ER/PM association will occur in the native condition as the expression of both VAP27 and NET3C are limited (scale bar = 10μm).

209x297mm (300 x 300 DPI)

Figure 8

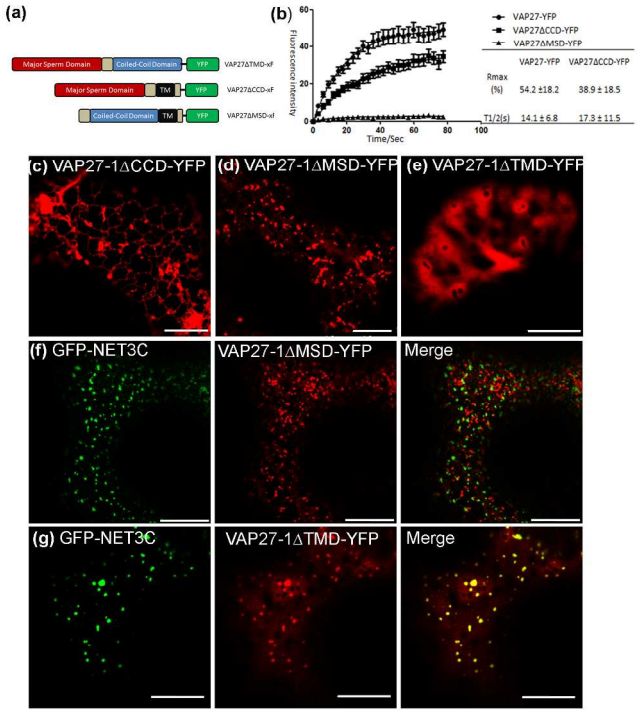

Figure 8. Localisation and dynamics of VAP27 domain deletion mutants in transiently transformed N. benthamiana leaf epidermal cells.

(a) Diagrammatic illustration of the fluorescent protein fusions of VAP27 or VAP27 deletion mutants used in this study. (b) Protein dynamics within the ER/PM contact site or punctate structures analysed using FRAP. The mobility of full length VAP27-1 is much greater (Rmax = 54.2 ± 18.2%) than the coiled-coil domain deletion mutants (Rmax = 38.9 ± 18.5%). The punctae induced by VAP27-1ΔMSD exhibited little recovery during the time course (c) VAP27-1 without the coil-coiled domain (ΔCCD) localises to the ER network. Punctate structures still formed at the ER nodules, and the morphology of the ER does not change significantly. (d) VAP27-1 without the major sperm domain (ΔMSD) forms ER associated protein aggregates, which are very mobile. (e) VAP27 without the transmembrane domain (ΔTMD) distributed to the cytoplasm. It did not localise to the PM, which indicates that the transmembrane domain is essential for ER targeting as well as for PM interaction. (f) Punctate structures labelled by VAP27-1ΔMSD-YFP (red) did not co-localise with GFP-NET3C (green), indicating that they are unlikely to be the ER/PM contact sites and that the major

sperm domain is required for VAP27-NET3C interaction. (g) VAP27-1ΔTMD-YFP (red) is recruited from the cytoplasm to PM when co-expressed with NET3C (green; scale bar = 10μm).

209x297mm (300 x 300 DPI)

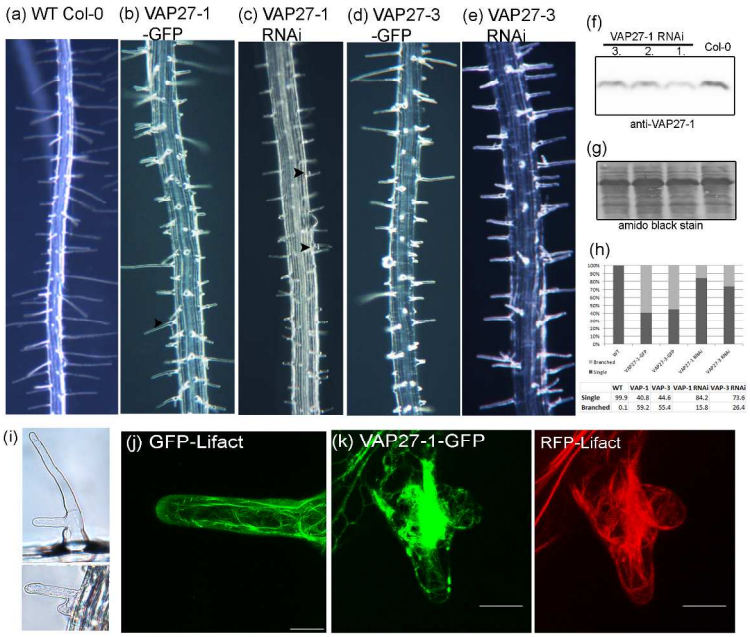

Figure 9. The change in the level of expression of VAP27 in Arabidopsis leads to developmental defects in root hairs.

(a) Root hairs found within the differentiation zone of wild type Arabidopsis. (b) The root hairs from VAP27-1 expressing Arabidopsis lines exhibit an abnormal phenotype. They are much shorter and swollen compared to the wild type, and most are branched. (c) Brached root hairs were also seen in VAP27-1 RNAi lines (arrow), suggesting that either over- or under-expression of VAP27 affects root hair development. (d-e) The branched root hair phenotype is also observed in VAP27-3 expressing and VAP27-3 RNAi plants. (f) Western blot of VAP27-1 RNAi Arabidopsis (1-3) and wild type, the knock-down of VAP27-1 protein was confirmed in these RNAi lines. (g) Amido black staining suggested equal amount of proteins were loaded in all lanes (lower panel). (h) Statistical analysis of branched root hairs in VAP27-1 and 3 over-expression or knock-down lines. The percentage for each line is shown in the table. (i) Branched root hairs at high magnification, two root hairs were often seen bulged from one trichoblast cell. (j) The actin cytoskeleton (labelled by GFP-Lifact) in a wild type root hair cell, with fine filaments in the apical part and thick bundles at the base (3D

maximum projection). (k) In the VAP27-1 expressing root hair cells, the ER and F-actin form aggregates, which affect its polarised growth. Instead of growing directionally, the root hair cell branched at the point where the membrane aggregates assemble (3D maximum projection; scale bar = 10μm).

209x297mm (300 x 300 DPI)